ARTICLE

Received 00th January 20xx,
Accepted 00th January 20xx

DOI: 10.1039/x0xx00000x

In-situ molecular compensation in wide-bandgap perovskite for efficient all-perovskite tandem solar cells

Sheng Fu, [+*a] Nannan Sun, [+a] Shuaifeng Hu, [+b] Hao Chen,*[c] Xinxin Jiang,[d] Yunfei Li,[a] Xiaotian Zhu,[a] Xuemin Guo,[a] Wenxiao Zhang,[a] Xiaodong Li,[a] Andrey S. Vasenko,[d] and Junfeng Fang*[a]

Substantial V_{OC} loss and halide segregation in wide-bandgap (WBG) perovskite sub-cells pose significant challenges for advancing all-perovskite tandem solar cells (APTSCs). Regarding this, one of the most impactful developments is the application of hole-selective self-assembled monolayers (SAMs), leading to the advancement in APTSC technology. However, SAMs with poor polar-solvent resistance would be inevitably delaminated from substrates during perovskite precursor coating, remaining great challenge in achieving a complete SAMs coverage with derivatization issues, e.g. defective perovskite and considerable interface energy loss. Here, we introduced an in-situ molecular compensation strategy to address the inherent flaw of SAMs within WBG perovskites via incorporating 5-ammonium valeric acid iodide (5-AVAI). The larger-dipole 5-AVAI spontaneously accumulates toward the buried interface to compensate the SAMs-deficient sites when depositing WBG perovskite, effectively minimizing interfacial energy loss. Simultaneously, amphoteric 5-AVAI with amino and carboxyl groups can compensate the defects at grain boundaries for solid passivation. Consequently, a champion efficiency of 20.23% with a record V_{OC} of 1.376 V was realized on WBG devices, enabling an efficiency of 28.9% for the APTSCs. Encouragingly, the tandems showed good operational stability and retained 87.3% of their efficiency after 800 hours of tracking.

Introduction

Monolithic all-perovskite tandem solar cells (APTSCs) stacking the wide bandgap (WBG, E_g approximately 1.8 eV) and narrow-bandgap (NBG, E_g approximately 1.25 eV) perovskite sub-cells have demonstrated potentials to overcome the Shockley-Queisser efficiency limit of single-junction perovskite solar cells (PSCs), attributed to the reduced charge carrier thermalization loss.[1-8] Considerable progresses have been made in both efficiency and stability of APTSCs over the past seven years.[9-12] Despite the rapid developments, the two inherent shortcomings of WBG top cell still hinder the step toward desirable APTSCs: *1.* the serious non-radiative recombination and interfacial energy losses cause large V_{OC} deficit (E_g-V_{OC});[11,13-15] *2.* lattice defects provide the channels for halide anion migrations and phase separation under photoelectric stresses.[16-18] Great efforts have been directed to minimize the V_{OC} losses and suppress photo degradations in WBG PSCs, such as crystallization optimizations,[13,19] defect regulations and surface capping with molecular passivation and two-dimension perovskite,[11,14,20-23] leading to the effective ameliorations. Considering the V_{OC} deficit of the best-in -class WBG cells (>0.45 V), however, there is still large room for improvement compared to that (at about 0.30 V) of the state-of-the-art cells with lower bandgaps.[24-26]

The successful application of self-assemble monolayers (SAMs) as the hole transport layers (HTLs) has been regarded as a milestone in inverted PSCs developments, where the SAMs provide desirable interface contacts for perovskite deposition and superior hole extraction, making them popular among the recorded inverted PSCs,[27-29] including recent state-of-the-art WBG ones.[11,26,30] Whereas the SAMs has been proved with erratic interfacial properties owing to incomplete coverage on the substrates, derivatizing undesirable issues, e.g. uneven crystallization with massive defects formation and considerable interface energy loss, thereby limiting the V_{OC} and stability of the devices.[31-36] Ex-situ regulations on the aggregation states in precursor and deposition kinetics of SAMs have shown ameliorations on the coverages.[16,23,26,37,38] Nevertheless, SAMs with poor polar-solvent resistance would be partially delaminated from substrates during perovskite precursor coating, leaving the inevitable origination for the incomplete coverage issues.[32] Resolving the incomplete issue of SAMs during perovskite coating

[a.] *School of Physics and Electronic Science, Engineering Research Center of Nano-photonics and Advanced Instrument Ministry of Education, East China Normal University, Shanghai 200062, China. E-mail:* sfu@phy.ecnu.edu.cn, jffang@phy.ecnu.edu.cn
[b.] *Clarendon Laboratory, Department of Physics, University of Oxford, Oxford OX1 3PU, UK.*
[c.] *Global Institute of Future Technology (GIFT), Shanghai Jiao Tong University, Shanghai 200240, China. E-mail:* hao.chen1@sjtu.edu.cn
[d.] *HSE University, Moscow 101000, Russia*
[+.] *These authors contribute equally to this work*
† Footnotes relating to the title and/or authors should appear here.
Supplementary Information available: [details of any supplementary information available should be included here]. See DOI: 10.1039/x0xx00000x

must provide the promising pathway to further reduce V_{OC} deficit in WBG PSCs for advanced APTSCs.

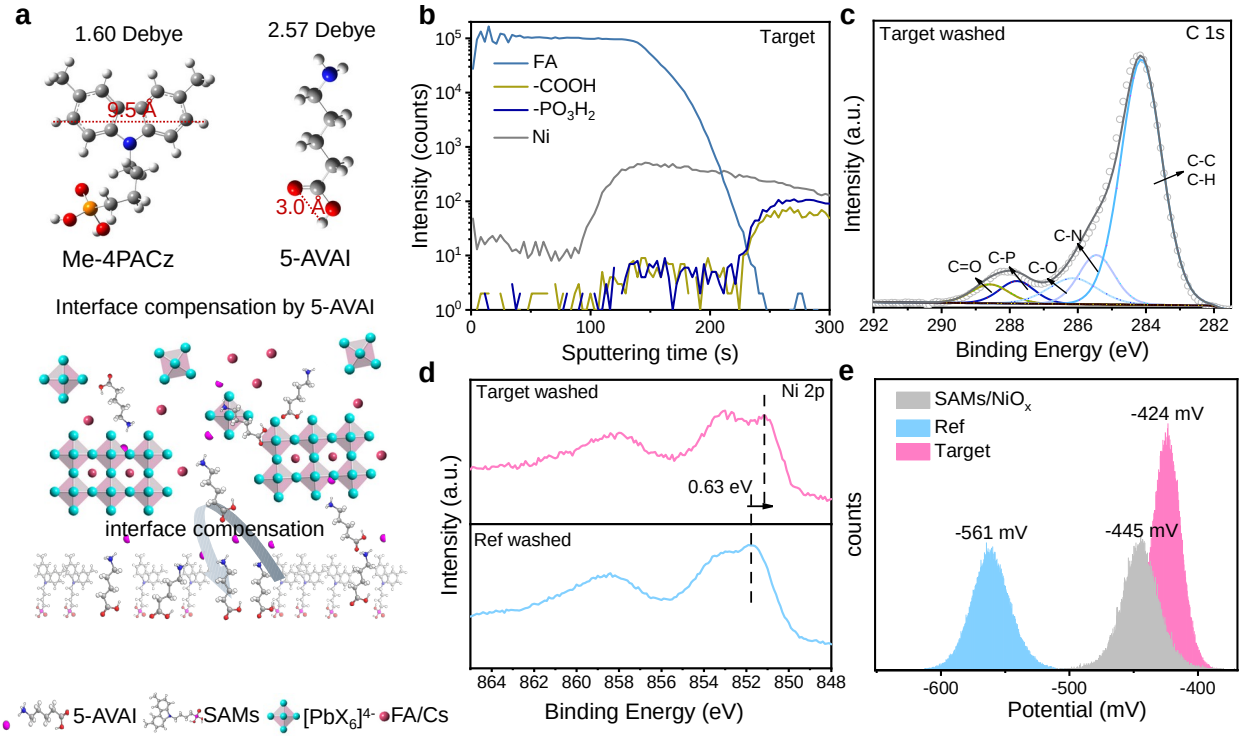

Fig. 1 Interface compensations via 5-AVAI. (a) Molecule structures and schematic diagram of the interface compensation via 5-AVAI during WBG perovskite deposition. (b) TOF-SIMS of the target film. (c-e) C 1s XPS (c), Ni 2p XPS (d) and KPFM results (e) of the DMF washed Ref and Target perovskite substrates.

Herein, we reported the in-situ molecular compensation strategy to compensate the incomplete-SAMs-coverage issues in WBG PSCs via simply incorporating 5-aminovaleric acid hydroiodide (5-AVAI) into precursor. During perovskite coating, larger-dipole 5-AVAI molecules spontaneously sediment into bottom regions, and compensated the SAMs-deficient nickel oxide (NiO_x) surface with the strong coordination/hydrogen bonds, effectively minimizing the interface energy losses. Simultaneously, the amphoteric 5AVAI molecules with amino and carboxyl groups can compensate the defective grain boundaries (GBs) for solid passivation during films annealing, functionally eliminating the harmful ions channels for solid passivation. The resulted WBG PSCs realized the champion efficiency of 20.23% with V_{OC} of 1.376 V (corresponding to a record V_{OC} deficit of 0.414 V, Table S1, ESI†), and retained 86.4% efficiency after maximum power point tracking (MPPT) under 1-sun illuminated for 600 h, surpassing the bare ones with low efficiency of 17.5% and inferior operational tolerance. When stacking with 1.25-eV NBG sub-cell, the APTSCs achieved the efficiency of up to 28.9% with a V_{OC} of 2.183 V and good operational stability with 87.3% maintaining after MPPT for 800 h

Results and discussion

Molecular structure plays a crucial role in interfacial compensation during perovskite coating.[33] For instance, a small horizontal diameter is essential to minimize spatial potential resistance and ensure adequate absorbance, while a strong anchoring group facilitates rapid compensation on SAMs-deficient areas. The straight-chain 5-AVAI molecule presented much smaller horizontal diameter (3 Å) in comparison to the conjugated (4- (3,6-dimethyl-9H-carbazole-9-yl) butyl) phosphonic acid (Me-4PACz) as illuminated in **Fig. 1a** (details in Fig. S1, ESI†). Meanwhile, the carboxyl group of 5AVAI molecules featured a strong chelating strength on the NiO_x, with the bonding energy of 0.767 eV (theoretical results in Fig. S2, ESI†), which would predominantly settle to bottom region of perovskite films for compensation during solvent evaporation as the schematic diagram illuminating in Fig. 1a bottom.[10,39-41] In good consistence, as seen in **Fig. 1b,** the signals of -COOH from time-off light secondary ion mass spectrometry (TOF-SIMS, the bare films labelled as Ref in Fig. S3, ESI†) exhibited the similar trend as the Me-4PACz with a remarkable aggregation around the buried interface areas, experimentally confirming the compensation effects of 5-AVAI. In addition, the 5-AVAI anchoring on bottom can donate larger dipole (2.57 Debye) compared to that (1.60 Debey) of the Me-4PACz, boosting to the hole extractions with less interface energy loss.

To further quantify the interface compensation, we removed the perovskite films by DMF washing, and evaluated the chemical bonding conditions changes with X-ray photoelectron spectroscopy (XPS). In comparison to the washed Ref (Fig. S4, ESI†), the sample with 5-AVAI (named as Target, **Fig. 1c**) exhibited the obvious -C=O signals at 288.6 eV after washed, corresponding to the unremoved 5-AVAI even washed by polar-solvent DMF. As seen in **Fig. 1d**, a chemical shift toward lower binding energy of 0.65 eV on Ni 2p orbital XPS was detected when comparing the Ref and Target, directly proving the desirable compensation of 5-AVAI by solid anchors on NiO_x.

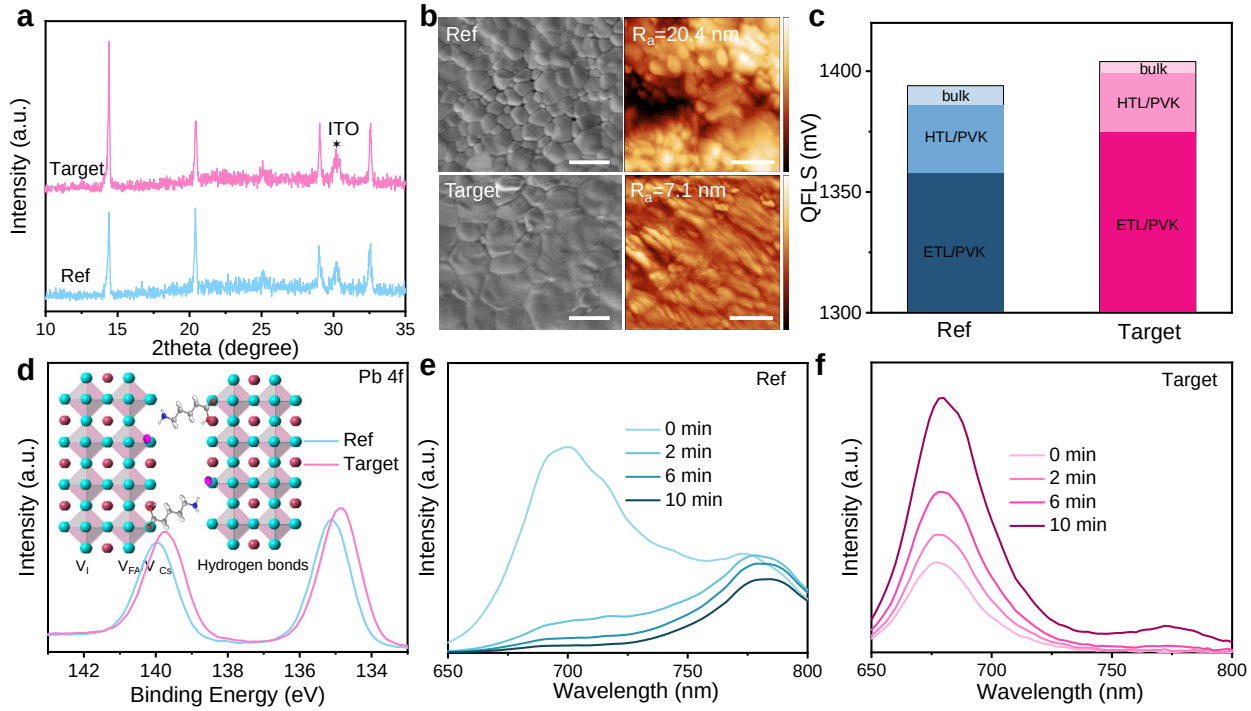

Fig. 2 Bulk defect compensations with 5-AVAI. **(**a-c) XRD patterns (a), SEM and AFM images (b), and QFLS values (c) of the Ref and Target WBG perovskite films. Inset bar of SEM and AFM images is 1 μm. **(**d) Pb 4f XPS spectra of the Ref and target films. (e-f) PL curves of the Ref (e) and target (f) films after 1-sun 532 nm laser exposure for different time.

The Kelvin probe force microscopy (KPFM, images in Fig. S5, ESI†) measurements were conducted on the SAMs/NiO_x and DMF-washed perovskite films to estimate the interface energy level differences, where the surface potential (SP_{mean}) values were plotted in **Fig. 1e**. The washed Ref film showed the lower SP_{mean} than the bare SAMs/NiO_x substrates, in good consistence to the reported delamination issue of SAMs during perovskite coating due to their poor polar-solvent resistance.[32] In contrast, the compensating with larger-dipole 5-AVAI resulted in the more p-type nature, with an improved potential and narrower distribution in comparison to the SAMs substrate, benefiting to minimizing interface loss for higher V_{OC}.[42,43]

The interaction between 5-AVAI and perovskite in the precursor film can regulate the nucleation and growth for highly crystalline WBG perovskite. The hydrogen proton nuclear magnetic resonance (H^1NMR, Fig. S6, ESI†) and Fourier transform infrared spectroscopy (FTIR, Fig. S7, ESI†) of the mixtures reveal the apparent chemical shift in comparison to the pure compounds, directly uncovering the formation of the hydrogen and coordination bindings between 5-AVAI and perovskite. **Fig. 2a** showed the X-ray diffraction (XRD) patterns of the Ref and Target, where we observe notable improvement in the peak intensity of the perovskite phase compared to the Ref without additional new phase detected. This indicates that the additional 5-AVAI had no effects to the crystal structure of perovskite and mainly located at the buried interface and grain boundaries (GBs) for compensations. This also provides the perovskite films with a maintained bandgap at 1.79 eV (Fig. S8, ESI†). The Target film presented the stronger XRD intensity than Ref, meaning the promoted crystallinity with 5-AVAI incorporation. **Fig. 2b** displayed the morphological investigations on the WBG perovskite films. The Ref film presented the inferior crystallization with uneven grain size and apparent pinholes from the top-view scanning electronic microscope (SEM) images, while the atomic force microscope (AFM) exhibited a large depression with surface roughness of 20.4 nm. In sharp contrast, the Target ones showed compact morphology with enhanced grain sizes and minimized surface roughness (7.4 nm), which benefits to the depositions of bottom LBG perovskite sub-cells during tandem fabrications.[44]

Benefitting from the improved crystal quality and effective passivation of 5-AVAI additive, we observe a 4-folder increase in the photoluminescence (PL) emission and 2-time elongation of carrier lifetime for target films from the Ref (Fig. S9, ESI†), suggesting a suppressed non-radiative recombination events. The trap density (N_t) in perovskite films is also reduced from an initial 1.01×10^{16} to 7.99×10^{15} cm^{-3} up on the addition of 5-AVAI (Fig. S10, ESI†). The PL quantum yield (PLQY, Fig. S11, ESI†) values of the pure perovskite films, perovskite/HTLs and perovskite/C_{60} are collected to estimate the VOC losses,[26,45] and the calculated quasi-Femi level splitting (QFLS) are plotted in **Fig. 2c**. Benefitting from promoted crystallization and defect passivation by 5-AVAI, the target shows higher QFLS than the Ref from both bulk and interfaces, indicating the suppression of V_{OC} deficits via molecular compensation.

The lattice vacancies are notorious as the main originations for the light-induced phase segregation in WBG perovskite with over 20% Br,[23,46,47] where vacancy sites provide the most channels for the migration of ions that are pronounced at defective GBs regions.[48] The 5-AVAI molecule bearing carboxyl and ammonium groups can effectively compensate the V_I and V_{Cs}/V_{FA} sites, respectively, to restrain the ion migration (**Fig. 2d** inset). The target film displays a –C=O peak in C 1s XPS spectra, without same signal detected in the

Ref (Fig. S12, ESI†). The interaction between 5-AVAI and perovskite lattices is further confirmed, evident from the obvious shifts to the lower and higher binding energy for Pb and halide core levels, respectively (Figs. 2d and S12c-d, ESI†).

achieved in the study is 1.376 V with a V_{OC} deficit of 0.414 V (Fig. S15, ESI†), representing the highest value among the reported WBG PSCs (Table S1, ESI†), to our best knowledge. The current densities obtained by integrating the external quantum efficiency (EQE, **Fig. 3b**) spectra with AM1.5 spectrum are 17.26 and 17.50 mA/cm^2 for Ref and target cells, respectively. The enhanced EQE response for target cells also suggests an improved film quality and charge carrier dynamics. 30 individual devices for each condition were taken into statistics (Figs. S16 and **3c**, ESI†). The narrow distributions of J–V parameters suggest a good reproducibility of devices, and the remarkable improvement in mean V_{OC} leads to a considerable increase of mean efficiency.

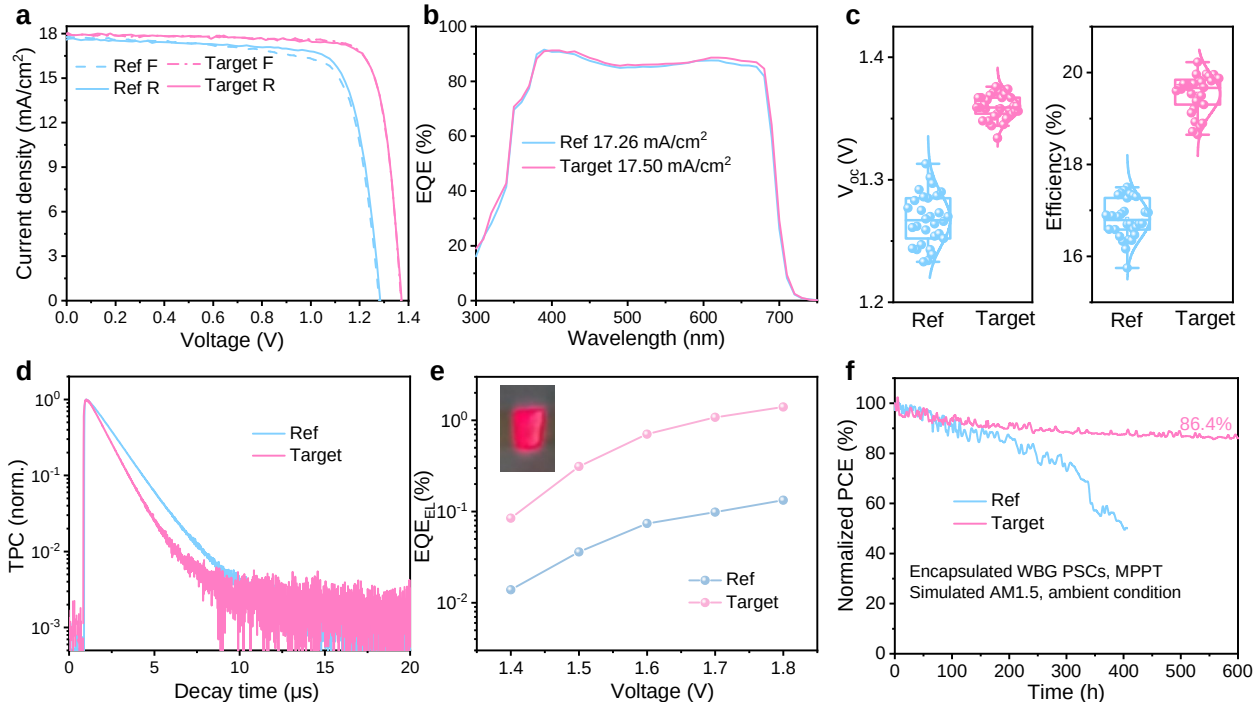

Fig. 3 Photovoltaic performance and stability of WBG PSCs. (a-f) J-V curves (a), EQE curves (b), parameters statistics (c), TPC curves (d), EL curves (e) and MPPT stability (f) of the corresponding WBG PSCs.

To evaluate the film stability, the toluene solutions containing WBG perovskite films are aged at simulated AM 1.5 illumination under 85 °C. The solution with Ref films exhibits a fast decomposition with the presence of I_3^- signals at 6 h and significantly increased absorption at 24 h **(**Fig. S13, ESI†**)**. On the contrary, the target samples show superior durability with much lower concentration of I_3^- generated after the same operations as the Ref. To further verify the improved stability of the films, we measure the spectrum stability with the films exposed under the illumination of a 532 nm laser with a 1-sun equivalent intensity (PL mappings in Fig. S14, ESI†). The phase segregation was detected with an I-rich PL emission at 783 nm appearing in the Ref during the first PL mapping collection (set as 0 min, **Fig. 2e**), and more I-rich phase with stronger PL emission are largely separated from the 1.79-eV phase under further soaking. In sharp contrast, the target samples show superior durability and retain strong 1.79-eV emission (**Fig. 2f**) after ageing for 10 min under the same condition.

We fabricated the inverted WBG PSCs with a configuration of ITO/NiO_x/Me-4PACz/perovskite/C60/ALD-SnO_2/Ag and the J-V curves of the champion efficiency were plotted in **Fig. 3a** (detailed parameters in Table S2, ESI†). The Ref devices showed the champion efficiency of 17.5% with a big V_{OC} deficit of 0.505 V under reverse scan, and notable hysteresis. Whereas the target cells showed a champion efficiency of 20.23% with a V_{OC} of 1.372 V. The J–V cures also demonstrate negligible hysteresis with a steady-state power output of 20.05% (Fig. 3a inset). In addition, the high V_{OC}

Superior charge carrier extraction dynamics with less undesirable recombination in the solar cells have been widely accepted as the important indicator for performance optimization,[49,50] and consistent results are concluded with the accelerated decay of transient photocurrent (TPC, **Fig. 3d**) signal and prolonged transient photovoltage (TPV in Fig. S17, ESI†) lifetime when taking the target and Ref into comparison. To further quantify the improvements, the sun-V_{OC} dependent measurements (Fig. S18a, ESI†) were performed, and the fill factor (FF) loss analysis (Fig. S18b, ESI†) was fitted according to previous reports.[51-53] Incorporating 5-AVAI contributes to effectively reducing transport (from 6 to 3.58%) and non-radiative recombination losses (from 7.5 to 2.86%), highlighting the effective compensations of the 5-AVAI. The V_{OC} losses in the devices are further investigated by operating as light-emitted diode (Fig. S19, ESI†), and the V_{OC} enhancement can be calculated with the electroluminescence (EL) EQE (**Fig. 3e**).[25] The fitted V_{OC} improvement is 60 mV, slightly lower than the 87 mV observed in the J-V curves, likely due to the absence of an integrated sphere during electroluminescence (EL) measurements.

Incorporating 5-AVAI not only enhanced device efficiency but also significantly prolonged their operational lifetime under simulated AM 1.5 illumination. As shown in **Fig. 3f**, the Ref PSCs present poor operational stability and lost over 50% of their initial efficiency after 400 h MPPT; whereas the target cells retain 86.4% of their initial efficiency after 600 h operation.

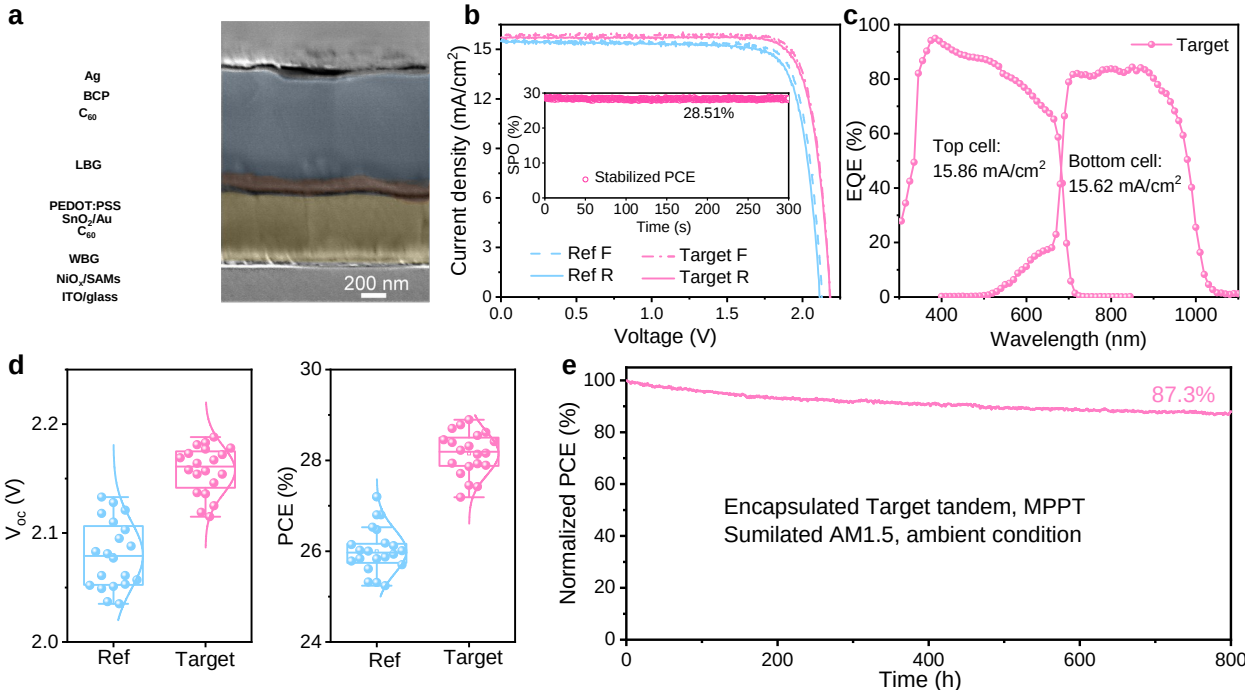

Fig. 4 Photovoltaic performance and stability of the APTSCs. a) Cross-sectional SEM image of the APTSCs. b-c) J-V curves (b), EQE spectra (c), parameters statistics (d) and MPPT result (e) of the APTSCs.

We fabricated the APTSCs by stacking the WBG perovskite sub-cells and the NBG Sn-Pb bottom sub-cells with the structural diagram and the cross-sectional SEM image in **Fig. 4a** (raw SEM image in Fig. S20, ESI†). The photovoltaic performance of NBG sub-cell showed the efficiency of 22.01% (Fig. S21, ESI†). The J-V curves of the champion efficiency for Ref and target APTSCs were presented in **Fig. 4b** (detailed parameters in Table S2, ESI†). The Ref showed the champion efficiency of 27.2 % with a V_{OC} of 2.128 V, a J_{SC} of 15.53 mA/cm^2 and a FF of 82.3 %. Whereas the target exhibited the champion efficiency of 28.9 % with an improved V_{OC} of 2.183 V, which is one of the reported high-efficiency APTSCs (Table S1, ESI†). The champion target showed a stable steady-state power output efficiency of 28.51%. The current densities integrated from EQE measurements (**Fig. 4c**) were 15.86 and 15.62 mA/cm^2 for WBG and LBG subcells, respectively, well matched with the J_{SC} of 15.74 mA/cm^2 from J-V scanning.

The photovoltaic parameters statistics of the APTSCs were presented in **Fig. 4d** and Fig. S22 (ESI†). In comparison to the Ref tandems, the obvious improvements on V_{OC} (from 2.08 to 2.158 V) and FF (from 81.4% to 83.6) for the target ones contributed to the efficiency enhancement from 26% to 28.15%. Moreover, gathering the promoted crystallization and compensation effects of 5-AVAI, the target APTSCs showed good operational stability (**Fig. 4e**) and retained 87.3% of its initial efficiency after MPPT for 800 h in ambient condition.

Conclusions

In summary, facing on the V_{OC} loss and device stability issues caused by SAMs-delamination issue in WBG sub-cells, we have demonstrated an effective strategy of in-situ molecular compensation during perovskite coating via the 5-AVAI incorporation. The 5-AVAI molecules with small horizonal size and large dipole spontaneously gather toward buried interface during WBG perovskite deposition, effectively compensating the SAM-absence sites for less interfacial energy loss. Furthermore, the amphoteric 5-AVAI compensate the defects at grain boundaries with strong interactions to stabilize the annealing WBG films. The resulted WBGs achieved the champion efficiency of 20.23% with a record V_{OC} of 1.376 V and improved stability. A champion efficiency of 28.9% was realized after stacking with a NBG perovskite sub-cells for APTSCs, and the tandem remained 87.3% of its initial efficiency after MPPT for 800 h in ambient condition.

Author contributions

SF and JF conceived the strategy. SF and NNS fabricated WBG and tandem devices. NNS, SFH and HC conducted the film fabrications and characterizations. XJ and ASV performed the DFT simulations. SF performed stability tests. YFL and XTZ took the XRD and PL measurements. XMG, WXZ and XDL conducted the TOF-SIMS depth profiles. SF, SFH and JF wrote the first draft of the manuscript. SF, HC, SFH and JF edited the manuscript. JF supervised

the projects and process. All authors discussed and contributed to the revision of the manuscript.

Conflicts of interest

There are no conflicts to declare.

Acknowledgements

This work was supported by the National Science Fund for Distinguished Young Scholar (T2325011), National Natural Science Foundation of China (62274062, 62374058, 52173161, 62104070), the Fundamental Research Funds for the Central Universities, Shanghai Science and Technology Innovation Action Plan (22dz1205200), Natural Science Foundation of Shanghai (22ZR1420000), Key Fundamental Research Project funding from the Shenzhen Science and Technology Innovation Committee (Grant No. KCXST20221021111616039) and National Youth Top-notch Talent Support Program.

References

1. S. Hu, J. Thiesbrummel, J. Pascual, M. Stolterfoht, A.Wakamiya, H. J. Snaith, *Chem. Rev.,* 2024, **124**, 4079.
2. X. Zheng, A. Y. Alsalloum, Y. Hou, E. H. Sargent, O. M. Bakr, *Acc. Mater. Res.,* 2020, 1, 63.
3. Z. Yu, Z. Yang, Z. Ni, Y. Shao, B. Chen, Y. Lin, H. Wei, Z. J. Yu, Z. Holman, J. S. Huang, *Nat. Energy,* 2020, **5**, 657.
4. E. Aydin, E. Ugur, B. K. Yildirim, T. G. Allen, P. Dally, A. Razzaq, F. Cao, L. Xu, B. Vishal, A. Yazmaciyan, A. A. Said, S. Zhumagali, R. Azmi, M. Babics, A. Fell, C. Xiao, S. De Wolf, *Nature* 2023, **623**, 732.
5. S. De Wolf, E. Aydin, *Science,* 2023, **381**, 30.
6. Q.-Q. Chu, Z. Sun, J. Hah, K.-s. Moon, B. Cheng, D. Wang, P. Xiao, Y. Zhou, A. Petrozza, G.-J. Yang, H. Wang, C.-P. Wong, *Mater. Today,* 2023, **67**, 399.
7. C. Wang, Y. Zhao, T. Ma, Y. An, R. He, J. Zhu, C. Chen, S. Ren, F. Fu, D. Zhao, X. Li, *Nat. Energy,* 2022, **7**, 744.
8. R. He, W. Wang, Z. Yi, F. Lang, C. Chen, J. Luo, J. Zhu, J. Thiesbrummel, S. Shah, K. Wei, Y. Luo, C. Wang, H. Lai, H. Huang, J. Zhou, B. Zou, X. Yin, S. Ren, X. Hao, L. Wu, J. Zhang, J. Zhang, M. Stolterfoht, F. Fu, W. Tang, D. Zhao, *Nature,* 2023, **618**, 80.
9. H. Gao, K. Xiao, R. Lin, S. Zhao, W. Wang, S. Dayneko, C. Duan, C. Ji, H. Sun, A. D. Bui, C. Liu, J. Wen, W. Kong, H. Luo, X. Zheng, Z. Liu, H. Nguyen, J. Xie, L. Li, M. I. Saidaminov, H. Tan, *Science,* 2024, **383**, 855.
10. S. Zhou, S. Fu, C. Wang, W. Meng, J. Zhou, Y. Zou, Q. Lin, L. Huang, W. Zhang, G. Zeng, D. Pu, H. Guan, C. Wang, K. Dong, H. Cui, S. Wang, T. Wang, G. Fang, W. Ke, *Nature,* 2023, **624**, 69.
11. H. Chen, A. Maxwell, C. Li, S. Teale, B. Chen, T. Zhu, E. Ugur, G. Harrison, L. Grater, J. Wang, Z. Wang, L. Zeng, S. M. Park, L. Chen, P. Serles, R. A. Awni, B. Subedi, X. Zheng, C. Xiao, N. J. Podraza, T. Filleter, C. Liu, Y. Yang, J. M. Luther, S. De Wolf, M. G. Kanatzidis, Y. Yan, E. H. Sargent, *Nature,* 2023, **613**, 676.
12. S. Fu, N. Sun, Y. Xian, L. Chen, Y. Li, C. Li, A. Abudulimu, P. N. Kaluarachchi, Z. Huang, X. Wang, K. Dolia, D. S. Ginger, M. J. Heben, R. J. Ellingson, B. Chen, E. H. Sargent, Z. Song, Y. Yan, *Joule,* 2024, **8**, 2220.
13. X. Meng, X. Liu, Q. Zhou, Z. Liu, W. Chen, *Nano Energy,* 2024, **128**, 109984.
14. S. Wu, Y. Yan, J. Yin, K. Jiang, F. Li, Z. Zeng, S.-W. Tsang, A. K. Y. Jen, *Nat. Energy,* 2024, **9**, 411.
15. X. Jiang, Q. Zhou, Y. Lu, H. Liang, W. Li, Q. Wei, M. Pan, X. Wen, X. Wang, W. Zhou, D. Yu, H. Wang, N. Yin, H. Chen, H. Li, T. Pan, M. Ma, G. Liu, W. Zhou, Z. Su, Q. Chen, F. Fan, F. Zheng, X. Gao, Q. Ji, Z. Ning, *Natl. Sci. Rev*., 2024, **11**, nwae055.
16. J. Wen, Y. Zhao, P. Wu, Y. Liu, X. Zheng, R. Lin, S. Wan, K. Li, H. Luo, Y. Tian, L. Li, H. Tan, *Nat. Commun.,* 2023, **14**, 7118.
17. C. Liu, Y. Yang, H. Chen, J. Xu, A. Liu, A. S. R. Bati, H. Zhu, L. Grater, S. S. Hadke, C. Huang, V. K. Sangwan, T. Cai, D. Shin, L. X. Chen, M. C. Hersam, C. A. Mirkin, B. Chen, M. G. Kanatzidis, E. H. Sargent, *Science,* 2023, **382**, 810.
18. T. T. Li, J. Xu, R. X. Lin, S. Teale, H. J. Li, Z. Liu, C. Y. Duan, Q. Zhao, K. Xiao, P. Wu, B. Chen, S. Jiang, S. B. Xiong, H. W. Luo, S. S. Wan, L. D. Li, Q. Y. Bao, Y. X. Tian, X. P. Gao, J. Xie, E. H. Sargent, H. R. Tan, *Nat. Energy,* 2023, **8**, 610.
19. L. Qiao, T. Ye, T. Wang, W. Kong, R. Sun, L. Zhang, P. Wang, Z. Ge, Y. Peng, X. Zhang, M. Xu, X. Yan, J. Yang, X. Zhang, F. Zeng, L. Han, X. Yang, *Adv. Energy Mater.,* 2023, **14**, 202302983.
20. S. Jiang, R. Wang, M. Li, R. Yu, F. Wang, Z. a. Tan, *Energy Environ. Sci.,* 2024, **17**, 219.
21. S. Fu, J. Le, X. Guo, N. Sun, W. Zhang, W. Song, J. Fang, *Adv. Mater.,* 2022, **34**, e2205066.
22. J. Zhu, Y. Luo, R. He, C. Chen, Y. Wang, J. Luo, Z. Yi, J. Thiesbrummel, C. Wang, F. Lang, H. Lai, Y. Xu, J. Wang, Z. Zhang, W. Liang, G. Cui, S. Ren, X. Hao, H. Huang, Y. Wang, F. Yao, Q. Lin, L. Wu, J. Zhang, M. Stolterfoht, F. Fu, D. Zhao, *Nat. Energy,* 2023, **8**, 714.
23. Q. Jiang, J. Tong, R. A. Scheidt, X. Wang, A. E. Louks, Y. Xian, R. Tirawat, A. F. Palmstrom, M. P. Hautzinger, S. P. Harvey, S. Johnston, L. T. Schelhas, B. W. Larson, E. L. Warren, M. C. Beard, J. J. Berry, Y. Yan, K. Zhu, *Science,* 2022, **378**, 1295.
24. M. Jeong, I. W. Choi, E. M. Go, Y. Cho, M. Kim, B. Lee, S. Jeong, Y. Jo, H. W. Choi, J. Lee, J. H. Bae, S. K. Kwak, D. S. Kim, C. Yang, *Science,* 2020, **369**, 1615.
25. Q. Jiang, Y. Zhao, X. Zhang, X. Yang, Y. Chen, Z. Chu, Q. Ye, X. Li, Z. Yin, J. You, *Nat. Photonics,* 2019, **13**, 460.
26. Y. Wang, R. Lin, C. Liu, X. Wang, C. Chosy, Y. Haruta, A. D. Bui, M. Li, H. Sun, X. Zheng, H. Luo, P. Wu, H. Gao, W. Sun, Y. Nie, H. Zhu, K. Zhou, H. T. Nguyen, X. Luo, L. Li, C. Xiao, M. I. Saidaminov, S. D. Stranks, L. Zhang, H. Tan, *Nature,* 2024**, 635**, 867-873.
27. M. Li, M. Liu, F. Qi, F. R. Lin, A. K. Jen, *Chem. Rev.* 2024, **124**, 2138.
28. H. Chen, C. Liu, J. Xu, A. Maxwell, W. Zhou, Y. Yang, Q. Zhou, A. S. R. Bati, H. Wan, Z. Wang, L. Zeng, J. Wang, P. Serles, Y. Liu, S. Teale, Y. Liu, M. I. Saidaminov, M. Li, N. Rolston, S. Hoogland, T. Filleter, M. G. Kanatzidis, B. Chen, Z. Ning, E. H. Sargent, *Science,*

2024, **384**, 189.

29. T. Duan, S. You, M. Chen, W. Yu, Y. Li, P. Guo, J. J. Berry, J. M. Luther, K. Zhu, Y. Zhou, *Science,* 2024, **384**, 878.
30. Z. Wei, Q. Zhou, X. Niu, S. Liu, Z. Dong, H. Liang, J. Chen, Z. Shi, X. Wang, Z. Jia, X. Guo, R. Guo, X. Meng, Y.-D. Wang, N. Li, Z. Xu, Z. Li, A. G. Aberle, X. Yin and Y. Hou, *Energy Environ. Sci.,* 2025, **18**, 1847-1855.
31. S. Yu, Z. Xiong, H. Zhou, Q. Zhang, Z. Wang, F. Ma, Z. Qu, Y. Zhao, X. Chu, X. Zhang, J. You, *Science,* 2023, **382**, 1399.
32. H. Tang, Z. Shen, Y. Shen, G. Yan, Y. Wang, Q. Han, L. Han, *Science,* 2024, **383**, 1236.
33. S. M. Park, M. Wei, N. Lempesis, W. Yu, T. Hossain, L. Agosta, V. Carnevali, H. R. Atapattu, P. Serles, F. T. Eickemeyer, H. Shin, M. Vafaie, D. Choi, K. Darabi, E. D. Jung, Y. Yang, D. B. Kim, S. M. Zakeeruddin, B. Chen, A. Amassian, T. Filleter, M. G. Kanatzidis, K. R. Graham, L. Xiao, U. Rothlisberger, M. Gratzel, E. H. Sargent, *Nature,* 2023, **624**, 289.
34. M. Liu, L. Bi, W. Jiang, Z. Zeng, S. W. Tsang, F. R. Lin, A. K. Y. Jen, *Adv. Mater.,* 2023, **35**, 202304415.
35. R. Guo, X. Wang, X. Jia, X. Guo, J. Li, Z. Li, K. Sun, X. Jiang, E. Alvianto, Z. Shi, M. Schwartzkopf, P. Müller-Buschbaum and Y. Hou, *Adv. Energy Mater.,* 2023, **13**, 2302280.
36. S. Fu, N. Sun, H. Chen, Y. Li, Y. Li, X. Zhu, B. Feng, X. Guo, C. Yao, W. Zhang, X. Li and J. Fang, *Energy Environm. Sci.,* 2025, **18**, 3305-3312.
37. F. Xu, E. Aydin, J. Liu, E. Ugur, G. T. Harrison, L. Xu, B. Vishal, B. K. Yildirim, M. Wang, R. Ali, A. S. Subbiah, A. Yazmaciyan, S. Zhumagali, W. Yan, Y. Gao, Z. Song, C. Li, S. Fu, B. Chen, A. ur Rehman, M. Babics, A. Razzaq, M. De Bastiani, T. G. Allen, U. Schwingenschlögl, Y. Yan, F. Laquai, E. H. Sargent, S. De Wolf, *Joule,* 2024, **8**, 224.
38. X. Wang, J. Li, R. Guo, X. Yin, R. Luo, D. Guo, K. Ji, L. Dai, H. Liang, X. Jia, J. Chen, Z. Jia, Z. Shi, S. Liu, Y. Wang, Q. Zhou, T. Wang, G. Pan, P. Müller-Buschbaum, S. D. Stranks and Y. Hou, *Nat. Photonics,* 2024, **18**, 1269-1275.
39. S. Hu, K. Otsuka, R. Murdey, T. Nakamura, M. A.Truong, T. Yamada, T. Handa, K. Matsuda, K. Nakano, A. Sato, et al. *Energy Environ. Sci.,* 2022, **15**, 2096-2107.
40. T. Ma, H.Wang, Z. Wu, Y. Zhao, C. Chen, X. Yin, L. Hu, F. Yao, Q. Lin, S. Wang, et al. *Adv. Mater.,* 2024, **36**, e2308240.
41. X. Li, X. Liu, X. Wang, L. Zhao, T. Jiu, J. Fang, *J. Mater. Chem. A,* 2015, **3**, 15024.
42. S. Liu, J. Li, W. Xiao, R. Chen, Z. Sun, Y. Zhang, X. Lei, S. Hu, M. Kober-Czerny, J. Wang, et al. *Nature,* 2024, **632**, 536-542.
43. D. Li, Q. Lian, T. Du, R. Ma, H. Liu, Q. Liang, Y. Han, G. Mi, O. Peng, G. Zhang, et al. *Nat. Commun.,* 2024, **15**, 7605.
44. Y. Wang, R. Lin, X. Wang, C. Liu, Y. Ahmed, Z. Huang, Z. Zhang, H. Li, M. Zhang, Y. Gao, H. Luo, P. Wu, H. Gao, X. Zheng, M. Li, Z. Liu, W. Kong, L. Li, K. Liu, M. I. Saidaminov, L. Zhang, H. Tan, *Nat. Commun.,* 2023, **14**, 1819.
45. J. Li, H. Liang, C. Xiao, X. Jia, R. Guo, J. Chen, X. Guo, R. Luo, X. Wang, M. Li, M. Rossier, A. Hauser, F. Linardi, E. Alvianto, S. Liu, J. Feng and Y. Hou, *Nat. Energy*, 2024, **9**, 308-315.
46. H. Zhang, X. Fu, Y. Tang, H. Wang, C. Zhang, W. W. Yu, X. Wang, Y. Zhang, M. Xiao, *Nat. Commun.,* 2019, **10**, 1088.
47. Y. Wang, X. Guan, W. Chen, J. Yang, L. Hu, J. Yang, S. Li, K. Kalantar-Zadeh, X. Wen, T. Wu, *ACS Appl. Mater. Interfaces,* 2020, **12**, 38376.
48. W. Li, M. U. Rothmann, A. Liu, Z. Wang, Y. Zhang, A. R. Pascoe, J. Lu, L. Jiang, Y. Chen, F. Huang, Y. Peng, Q. Bao, J. Etheridge, U. Bach, Y.-B. Cheng, *Adv. Energy Mater.,* 2017, **7**, 1700946.
49. J. Xu, A. Maxwell, Z. Song, A. S. R. Bati, H. Chen, C. Li, S. M. Park, Y. Yan, B. Chen, E. H. Sargent, *Nat. Commun.,* 2024, **15**, 2035.
50. H. Li, B. Chang, L. Wang, Y. Wu, Z. Liu, L. Pan, L. Yin, *ACS Energy Lett.,* 2024, **9**, 400.
51. W. Peng, K. Mao, F. Cai, H. Meng, Z. Zhu, T. Li, S. Yuan, Z. Xu, X. Feng, J. Xu, M. D. McGehee, J. Xu, *Science,* 2023, **379**, 683.
52. Z. Li, X. Sun, X. Zheng, B. Li, D. Gao, S. Zhang, X. Wu, S. Li, J. Gong, J. M. Luther, Z. Li, Z. Zhu, *Science,* 2023, **382**, 284.
53. L. Chen, C. Li, Y. Xian, S. Fu, A. Abudulimu, D. B. Li, J. D. Friedl, Y. Li, S. Neupane, M. S. Tumusange, N. Sun, X. Wang, R. J. Ellingson, M. J. Heben, N. J. Podraza, Z. Song, Y. Yan, *Adv. Energy Mater.,* 2023, **13**, 202301218.